Myocardial infarction triggers cardioprotective antigen-specific T helper cell responses

Authors: Max Rieckmann[1], Murilo Delgobo[2,3], Chiara Gaal[2,3], Lotte Büchner[2,3], Philipp Steinau[1], Dan Reshef[4], Cristina Gil-Cruz[5], Ellis N. ter Horst[6-9], Malte Kircher[10], Theresa Reiter[2], Katrin G. Heinze[11], Hans W. M. Niessen[7, 8], Paul A. J. Krijnen[7, 8], Anja M. vanderLaan[6], Jan J. Piek[6, 8], Charlotte Koch[1], Hans-Jürgen Wester[12], Constantin Lapa[10], Wolfgang R. Bauer[2], Burkhard Ludewig[5], Nir Friedman[4], Stefan Frantz[1, 2, 3†], Ulrich Hofmann[1, 2, 3†], Gustavo Campos Ramos[1, 2, 3†*]

Supplementary Materials:

This file includes:

Supplementary Materials and Methods

Animals: The mice were maintained in individually ventilated cages under specific pathogen-free (SPF) conditions with a 12-hour light/12-hour dark cycle and standard diet provided ad libitum and were enrolled in the MI studies at the age of 8-12 weeks. WT male BALB/c mice were commercially acquired from Charles River (stock # 028). As described by Nindl et al. (1), TCR-M mice expressing a transgenic TCR specific for a class-II-restricted cardiac myosin peptide ($MYHCA_{614-628}$) were bred in the housing facility at the University Hospital Halle after being kindly provided by Prof. Burkhard Ludewig. The TCR-M mice expressed the congenic marker Thy1.1, whereas the WT mice express Thy1.2. Lymphocyte-deficient $Rag1^{-/-}$ and DO11.10 mice (expressing a transgenic TCR specific for the irrelevant antigen $Ovalbumin_{323-339}$) were commercially acquired from Jackson (Stock # 003145 and 003303, respectively). All these mouse strains share the same genetic background (BALB/c). The mice were maintained in groups of two to six individuals and acclimatized for at least 7 days after shipment.

Experimental myocardial infarction (EMI) was induced under strict aseptic conditions after left coronary artery (LAD) permanent ligation, as previously described (2, 3). Briefly, under isoflurane (Forene, Abbott, Wiesbaden, Germany) anesthesia (initially 4%, maintenance at 2.0-2.5% vol/vol 0_2), the mice were intubated for mechanical ventilation and then subjected to thoracotomy. After skin shaving, disinfection (Braunoderm, B. Braun, Melsungen, Germany) and

incision, the third intercostal space was accessed by blunt preparation and held open by a microretractor. Following lung displacement using a Ringer lactate-soaked (Baxter, Unterschleißheim, Germany) piece of sponge (Pro-ophta, Lohmann & Rauscher, Rengsdorf, Germany), the LAD of the mice in the MI group was permanently ligated using 6/0 perma-hand silk thread (Ethicon, Norderstedt, Germany). This step was omitted in the sham operation. Success was rated by paling and akinesia of the tributary myocardium. The chest cage and skin were sutured sequentially using 5/0 and 6/0 Prolene thread, respectively (Ethicon). The isoflurane concentration was reduced to 0.5%, and the mice were extubated as soon as spontaneous respiration occurred. The body temperature was controlled during the operation, and the mice were subjected to a pain management program (buprenorphine s.c. 0.1 mg/kg body weight, Buprenovet, Bayer Vital, Leverkusen, Germany) 1 hour before and for at least 3 days (twice daily) after the operation. Endpoint analyses were performed on days 5, 7 and 49 postoperation. Echocardiography was performed on day 7 post-MI.

Cardiac peptide library

The murine cardiac epitopes tested in this study were selected after *in silico* simulations. First, heart-enriched proteins (defined as proteins that showed five-fold increased expression in the heart compared with that in all other organs) were selected based on data available from the Human Protein Atlas project (4), and the protein sequences were accessed from the Universal Protein Knowledgebase (5). The homologous murine proteins were subsequently selected, and the entire sequences were screened in silico to identify 15-mer peptides that exhibit high affinity for the I-A^d major histocompatibility complex-II pocket, according to the IEDB resources (6). The identified peptides were custom-synthesized by JPT Peptides (Berlin, Germany), diluted in dimethyl sulfoxide and stored at -80°C as single-use aliquots.

ELISPOT assay

The spleens from infarcted and sham-operated mice (day 7 postoperation) were collected and ground against a 30-µm filter mesh in serum-free C.T.L. medium to obtain a cell suspension, as previously described (7). Subsequently, 5 x 10^5 splenocytes were cultured in ELISpot plates in the presence of peptide pools comprising the selected proteins (each peptide at a concentration of 1 µg/ml, final DMSO concentration<0.05%) for 24 hours. The presence of IL-2- and IFN-γ-producing cells was monitored using commercially available ELISpot kits (C.T.L., Bonn, Germany) according to the manufacturer's instructions, and images were acquired using the Immunospot®S5 instrument (C.T.L., Bonn, Germany).

Echocardiographic assessments were performed with a Vevo 1100 instrument (VisualSonics, Amsterdam, Netherlands) coupled to a 30-MHz probe especially developed for mice, as previously described (2, 3). In brief, the mice were maintained under slight isoflurane anesthesia (0.5-1.5% vol/vol 0_2) on a heated bed (39°C), and images were acquired on the short axis (B-and M-mode) at midpapillary levels to represent the infarct border zones. All measurements were performed by an experienced veterinarian. The analyses were performed blinded using the manufacturer's software (Vevo® LAB 1.7.1), and only mice with a basal heart rate greater than 450 bpm were included in the analysis.

Adoptive cell transfers

Adoptive transfer of antigen-specific T helper cells into MI recipients: Myosin-specific $CD4^+$ T cells (Thy1.1) were purified from naïve TCR-M mice and then transferred into WT syngeneic recipients (Thy1.2) one day prior to the MI/sham operation. Accordingly, the TCR-M mice were sacrificed by cervical dislocation, and the spleen and lymph nodes (mandibular,

mesenteric, axillary, subiliac, mediastinal and popliteal) were aseptically extracted and stored in Hank's balanced salt solution containing 1% (vol/wt) bovine serum albumin (BSS/BSA). A cell suspension was obtained after the lymphoid organs were ground against a filter mesh (30 µm, Miltenyi Biotec, Bergisch-Gladbach, Germany) in BSS/BSA buffer. After an erythrocyte lysis step (RBC Lysis buffer, BioLegend, San Diego, CA, USA), untouched $CD4^+$ T cells were purified by magnetic cell sorting using the $CD4^+$ T cell Isolation Kit II (Miltenyi Biotec, Bergisch Gladbach, Germany). Finally, the TCR-M cells were resuspended in sterile PBS (Biochrom, Berlin, Germany) at a concentration of $2x10^7$ cells per ml and adoptively transferred into syngeneic recipient mice ($5x10^6$ cells i.p.) one day prior to MI induction (or sham operation). Baseline characterization of the donor cells and purity checks were routinely performed by flow cytometry. The in vivo distribution and phenotype of TCR-M cells in the recipients were monitored by flow cytometry based on the expression of the Thy1.1 congenic marker. To assess the effects of antigen-specific T helper cells on post-MI cardiac functionality, we also compared the effects of TCR-M and DO11.10 adoptive cell transfer ($1x10^7$, i.p.) into DO11.10 recipients. We selected DO11.10 recipients for this specific experimental setting to rule out the influence of endogenous heart-specific T helper cells.

Adoptive transfer of fluorescently labeled conventional and regulatory TCR-M cells into MI recipients: Conventional $CD4^+CD25^-$ T cells (Thy1.1) and regulatory $CD4^+CD25^+$ TCR-M cells were purified from spleen and LN samples obtained from naïve TCR-M mice. The Tconv cell fraction ($CD25^-$) was labeled with the intracellular fluorescent dye carboxyfluorescein succinimidyl ester (CFSE, Thermo Scientific, Darmstadt, Germany), whereas the Treg fraction ($CD25^+$) was labeled with CellTrace Violet (VIO, Thermo Scientific, Darmstadt, Germany). Briefly, after magnetic sorting, the cells were resuspended in a solution of 5 µM CFSE or VIO at a density of 10^6 cells/mL and incubated at 37°C for 20 minutes. Complete RPMI 1640 media plus

10% FCS was then added, and the cells were incubated for 5 minutes at 37°C. The cell suspensions were then washed, resuspended in sterile PBS and mixed at a Treg-to-Tconv ratio of 1:20. The labeled Treg/Tconv cells were adoptively transferred into syngeneic DO11.10 recipient mice (3x 10^6 cells i.p., 200 µl) one day prior to the EMI/sham operation. Baseline characterizations of donor cells and purity checks were performed by flow cytometry. Foxp3 staining showed a 15-fold enrichment of regulatory T cells in the $CD25^+$ fraction (Figure S1A). TCR-M cells were identified in vivo as $CD45^+CD4^+Thy1.1^+$ singlets in the analyzed cardiac and lymphoid tissues.

Adoptive transfer of MI-activated lymphocytes into lymphocyte-deficient mice: As a complementary approach, we also adoptively transferred lymphocytes purified from the med-LNs of MI or sham-operated mice into syngeneic lymphocyte-deficient mice ($Rag1^{-/-}$), as previously described (8). Thus, MI- and sham-operated WT mice were sacrificed 7 days postoperation, and their med-LNs were extracted in cold BSS/BSA. After the lymphoid organs were ground against a 30-µm cell strainer, lymphocytes were directly resuspended in sterile PBS at a concentration of $5x10^6$ cells per ml and then adoptively transferred into $Rag1^{-/-}$ recipients ($1x10^6$ bulk med-LN cells i.v.). Twenty-one days after transfer, the success of the transfer was assessed by flow cytometry, and cardiac echocardiography was performed 49 days post-transfer, one day prior to the endpoint analyses (organ extraction for cell culture and flow cytometry).

Endpoint analyses. At 5, 7 and 49 days post-MI/sham operation, the mice were sacrificed by cervical dislocation, whole-body perfusion with PBS was conducted, and the organs were extracted for *ex vivo* analyses. FACS analyses of freshly isolated cells (med-LN, si-LN, ax-LN, spleen and heart) were performed. The samples intended for RNA analysis were stored in RNA Later (Qiagen, Hilden, Germany) for 24 hours and then stored at -80°C, and the samples for histological analysis were embedded in Tissue-Tek® optimum cutting temperature medium (Sakura Finetek, Alphen aan den Rijn, The Netherlands) and then stored at -80°C.

Flow cytometry and fluorescence-activated cell sorting (FACS). Comprehensive immunophenotyping of med-LNs, si-LNs, spleens, and digested heart samples obtained from MI- and sham-operated mice were performed. The heart samples were enzymatically digested in type II collagenase (1,000 IU/ml, Worthington Biochemical Corporation, Lakewood, NJ, USA) for 30 minutes at 37°C and then ground against a 70-µm mesh (Miltenyi Biotec, Bergisch Gladbach, Germany) in BSS/BSA. The lymphoid organs were ground against a 30-µm cell strainer, and the splenocyte preparations underwent erythrocyte lysis. All the samples were resuspended in FACS buffer (PBS containing 1% BSA, 0.1% sodium azide and 1 mM EDTA). Surface staining was performed in the presence of FC-blocking antibody (anti-CD16/CD32, clone 2.4G2, BD Pharmingen) using the following antibody clones (conjugated with different fluorophores) commercially acquired from BioLegend (San Diego, CA, USA): anti-TCRß (clone H57-597), anti-TCR-Vα2 (clone B20.1), anti-CD4 (clone RM4-5 and GK1.5), anti-CD8a (clone 53-6.7), anti-Thy1.1 (clone OX-7), anti-CD44 (clone IM7), anti-CD11b (clone M1/70), anti-IA/IE (clone M5/114.15.2), anti-Ly6C (clone HK 1.4), anti-CCR2 (clone SA203G11), anti-CD64 (clone X54-5/7.1), anti-CXCR4 (clone I276F12), anti-Ly6G (clone 1A8), anti-TCRγ (clone GL3), anti-CD206 (clone C068C2), anti-CD25 (clone PC61), and anti-CD62L (clone MEL-14). In addition, AmCyan Zombie Aqua permeant was used for live/dead discrimination. Additionally, anti-CD45 (clone 30F11) and anti-Foxp3 (clone 150D/E4 and FJK-16s) antibodies were commercially acquired from BD and eBioscience, respectively.

In some experiments, TCR-M cells (defined as live $CD4^+TCRß^+Thy1.1^+TCR\text{-}Vα2^+$ singlets) were sorted from the med-LNs of MI- or sham-operated mice for gene expression profiling. The purity of the sorted cells was checked by flow cytometry, and only samples with >98% purity were used for downstream analyses. To obtain control cells, we also purified the

endogenous $CD4^+$ (defined as live $CD4^+TCR\beta^+Thy1.1^-$ singlets) compartment from the same mice. No sodium azide was included in the buffers for the samples intended for cell sorting.

Flow cytometry measurements were performed on LSRFortessa™ (BD Heildelberg, Germany) or on Attune-NxT (Thermo Scientific, Darmstadt, Germany), and all sorting experiments were performed using the BD-Aria-II (BD, Heildelberg, Germany). The analyses of flow cytometry data were performed using the Flowjo (Flowjo LLC Ashland, OR, USA). Compensation for spectral overlap was conducted based on single staining controls and the flow cytometry gates were set based on 'fluorescence minus one' (FMO) controls.

RNA purification and gene expression analyses: The RNA from sorted cells was purified using the RNeasy Plus Micro Kit (Qiagen, Düsseldorf, Germany) according to the manufacturer's instructions. The RNA quality was routinely monitored using the Agilent 2100 Bioanalyzer (Agilent Technologies, Waldbronn, Germany), and only samples with RIN above 8.0 were used for downstream applications.

A transcriptome analysis of 5-10x10^3 sorted $CD4^+$ T cells was conducted using GeneChip® WT Pico Reagent (Affymetrix, Santa Clara, CA, USA) according to the manufacturer's recommended protocol after the RNA was preamplified and its purity was assessed using a NanoDrop spectrophotometer (NanoDrop ND1000-Spectrophotometer, NanoDrop Technologies, Wilmington, DE, USA). The data were analyzed using the Affymetrix Expression Console (EC, 1.4.1.46, 2014) and Transcriptome Analysis Console (TAC, Version 3.0.0.466, 2014), as previously described (9). The enriched pathways and molecular functions of differentially expressed genes were analyzed on Enrichr, as previously described (10, 11).

Light-sheet fluorescence microscopy (LSFM) on wole unsliced murine hearts was conducted as previously described (8, 12). In brief, PBS-perfused whole hearts were fixated in 4% (wt/vol) formaldehyde (2 hours) and then washed in cold PBS. The hearts were then bleached in

15% (wt/vol) H_2O_2 in methanol for 30 minutes (murine hearts) of for 2 hours (human cardiac autopsies). The TCR-M cells infiltrating the infarcted myocardium were stained after the whole organs were incubated with anti-CD90.1 (clone OX-7) in PBS-Tween 20 buffer (0.05% vol/vol) for 5 days. The T cells in human cardiac autopsies (described below) were labeled using a polyclonal anti-CD3 (catalog # ab5690, Abcam, Bristol, UK). After washing and dehydration, the whole hearts were cleared with 1:3 benzyl alcohol/benzyl acetate (Sigma-Aldrich, Schnelldorf, Germany). Sequential multicolor stacks (1-mm total Z stack, 5-µm interval between images) of three to five hearts per group were imaged using a 5x objective lens. The autofluorescence on the green channel was recorded to acquire morphological information, and the images were processed and analyzed using Imaris software (Bitplane, Belfast, UK).

Histology: Heart cryosections (14 µm) from day 5 post-MI were fixed with 4% (vol/vol) formaldehyde in PBS and blocked with carbo-free solution (Vector Lab Inc. Burlingame, CA, USA) for 30 minutes and then stained with polyclonal anti-collagen III antibody (Catalog # PA5-27828 Invitrogen, 1:80) according to standard protocols that were previously established in our laboratory (2, 8). Phaloidin-A647 (Thermo Scientific, Darmstadt, Germany) was used for staining filamentous actin, which indicates a cardiomyocyte background. For picrosirius red staining (PSR, Morphisto, Frankfurt am Main, Germany), the cryosections were directly thawed in 4% (vol/vol) formaldehyde in PBS for 30 minutes and stained with PSR reagent (Morphisto, Frankfurt am Main, Germany) for 60 minutes. The sections were then washed with distilled water and dehydrated through consecutive passages in ethanol, xylol and Roti-Histol (Carl Roth, Karlsruhe, Germany). The green autofluorescence (Ex: 450-490 nm, Em: 500-550) was used to determine the morphology and area of the scar in the heart sections. The PSR fluorescence was analyzed using a “rhodamine” filter (Ex: 538-562 nm, Em: 570-640 nm) according to Vogel et al. (13). Uninjured remote areas were used as controls. The fluorescence images were acquired using an epifluorescence microscope

(model DFC 9000GT; Leica) coupled to a high-resolution camera (sCMOS monochrome fluorescence camera; Leica) and processed using ImageJ (NIH) software.

TCR sequencing. To assess the global impacts of MI on the T helper cell compartment, we purified $CD4^+$ T cells from the hearts and med-LNs of WT MI- and sham-operated mice and then performed downstream TCR sequencing. To determine whether the MI-related T cell repertoires are enriched in heart-specific TCR sequences, we also purified $CD4^+$ T cells from the ax-LNs of mice immunized s.c. with porcine cardiac myosin (100 µg, s.c. Sigma-Aldrich, Schnelldorf, Germany) or with a mouse heart protein extract (1 mg s.c., ax-LNs and si-LNs), both of which were emulsified in 200 or 600 µl of TiterMax Gold® (Sigma-Aldrich, Schnelldorf, Germany) as an adjuvant. The heart extract was obtained after mechanical homogenization (TissueRuptor, Qiagen) of whole hearts in PBS at a ratio of 1:15 (wt/vol), as previously described (14) and the total protein concentration was determined by the BCA method (Pierce, Waltham, MA, USA). As a control, we purified $CD4^+$ T cells from the ax-LNs of mice administered a 200-µl injection of the adjuvant only. FACS purification (day 7 post-MI or postimmunization), RNA isolation and quality checks were performed as described above. cDNA synthesis, library preparation and next-generation sequencing of TCRß complementary determining region 3 (CDR3) were performed by iRepertoire, Inc. (Huntsville, AL, USA) using an Illumina HiSeq platform. Bioinformatics analyses were performed at Friedman's laboratory using R software (Core Team, 2013), as previously described (15, 16). To normalize the differences in sample size across the tissue and LN samples, we used R sub-sampling "with replacement", and sub-sampled all repertoires to the same size (2.4M reads).

Cardiac autopsy samples

Patients, tissue collection and processing

This study was approved by and performed according to the guidelines of the ethics committee of Amsterdam UMC, location VUmc (Amsterdam Medical Center, Amsterdam, the Netherlands), which conformed to the Declaration of Helsinki. The use of leftover autopsy material for research following completion of the pathological examination is included in the patient contract of Amsterdam UMC. The current study included a total of 32 patients who were referred to the Department of Pathology of Amsterdam UMC, location VUmc, for clinical autopsy within 24 hours after death. Recent MI was diagnosed at autopsy using lactate dehydrogenase (LDH) decoloration as described previously (17). Twenty-three patients were diagnosed at autopsy with recent MI in the left ventricle. Nine patients who exhibited no pathological evidence of death from a cause related to MI were included as controls. Myocardial tissue specimens from MI patients were collected from the infarcted area, as identified by LDH decoloration. Tissue specimens from the control patients were collected from the left ventricle. All the tissue specimens were subsequently fixed in formalin and embedded in paraffin for immunohistochemical analysis. Based on the microscopic characteristics of the infarcted myocardium, MI patients were categorized into three different phases post-MI, as described in detail previously (17). Briefly, patients were considered to be in the early phase (~3-12 hours post-MI) if LDH decoloration was detected, but extravasation of neutrophilic granulocytes into the infarcted myocardium was not microscopically detectable (n=6). Patients were considered to be in the inflammatory phase (12 hours-5 days post-MI) if neutrophilic granulocytes had visibly infiltrated into the infarcted myocardium (n=9), and patients were considered to be in the proliferation phase (5-14 days post-MI) if granulation tissue was observed (n=8). Details are provided in Supplemental Table IV.

Immunohistochemistry

Deparaffinized and rehydrated sections of the myocardium were incubated in methanol/H_2O_2 (0.3%) for 30 minutes to block endogenous peroxidases. Antigen retrieval was performed by heating in Tris-EDTA buffer (pH 9.0). For Foxp3 single staining, the sections were incubated with mouse anti-human Foxp3 (1:100, clone 236A/E7, IgG1, eBioscience, ThermoFisher Scientific, Waltham, MA, USA). Subsequently, the Foxp3 antibody was labeled using the Brightvision-HRP kit (Immunologic, Duiven, the Netherlands) according to the manufacturer's recommended protocol. The staining complex was visualized using 3,3'-diaminobenzidine (DAB, 0.1 mg/ml, 0.02% H_2O_2, Dako, Copenhagen, Denmark). For CD4/Foxp3 double staining, the sections were incubated with rabbit anti-human CD4 (1:75, IgG, clone SP35, Spring Bioscience, Pleasanton, CA, USA) and mouse anti-human Foxp3 (1:25, clone 236A/E7 eBioscience). After washing with PBS, the sections were incubated for 30 minutes at room temperature (RT) with a Rabbit EnVision-HRP Detection Kit (Dako, Agilent, Santa Clara, CA, USA) to label CD4 immunostaining and with goat anti-mouse IgG1 biotin (1:100, Southern Biotech, Birmingham, AL, USA) to label Foxp3 immunostaining. Subsequently, the sections were incubated for 60 minutes at RT with streptavidin antialkaline phosphatase (AP) (1:100, Roche, Almere, the Netherlands) to label Foxp3-biotin. CD4 staining was visualized using DAB (0.1 mg/ml, 0.02% H_2O_2, Dako). Foxp3-biotin-streptavidin-AP was visualized using the alkaline phosphatase substrate and Fast Blue BB Base (Sigma-Aldrich, St. Louis, MO, USA). For this purpose, 10 mg of naphthol AS-MX phosphate (Sigma-Aldrich, St. Louis, MO, USA) was dissolved in 0.2 ml of dimethylformamide in a glass tube together with 40 ml of 0.2 M Tris/HCl buffer pH 8.5. Immediately prior to the use of this solution, 10 mg of Fast Blue BB Base was added to 0.25 ml of 2 N HCL and 0.25 ml of 4% $NaNO_2$, and the resulting mixture was mixed with the prepared alkaline phosphatase solution. Subsequently, 9.6 mg of levamisole (Sigma-Aldrich, St Louis, MO, USA) was added to 0.4 ml of 1 M $MgCl_2$, and the resulting mixture was filtered and

added directly to the slides for 45 minutes at RT. After washing with tap water, the slides were mounted using Aquatex® (Merck KGaA, Darmstadt, Germany), and the stained slides were scanned and analyzed manually using the Pannoramic Viewer program (version 1.15.4; 3DHistech Ltd., Budapest, Hungary).

Imaging studies in MI patients

German federal laws accept the use of the radiotracer [^{68}Ga]Pentixafor under the conditions of pharmaceutical law. All patients provided written informed consent prior to imaging.

Subjects and study design

[^{68}Ga]Pentixafor is a radiolabeled CXCR4-ligand for PET imaging (18-21), and the capability to specifically visualize human CXCR4 expression in various oncologic malignancies and inflammatory conditions was recently demonstrated (18-21). A portion of the patient cohort was previously described by Reiter et al. (21). Between January 2015 and June 2016, 22 patients with MI (17 males and five females, mean age of 61±11 years) underwent molecular imaging with [^{68}Ga]Pentixafor-PET/CT (PET/CT) as well as cardiac magnetic resonance (CMR; 21 patients, one excluded due to *adipositas permagna*). Thirteen patients returned after a median of 4 months for follow-up CMR imaging (range 1- 4 months).

Five patients (three males and two females; aged 59±8 years) who underwent CXCR4-directed PET/CT due to suspicion of benign Conn's adenoma were included as controls. Conn's adenomas are aldosterone-producing benign conditions that account for 30-40% of all cases of primary aldosteronism. Because these adenomas have been shown to overexpress CXCR4 (22), these patients were subjected to receptor-directed imaging as part of the endocrinological investigation. These patients had no malignancy and normal serum levels of C-reactive protein

(<0.5 mg/dl). Details are provided in Supplemental Table V. To the best of our knowledge, these patients represent the most suitable control group possible because the exposure of healthy volunteers to unnecessary radiation cannot be justified.

PET imaging

[^{68}Ga]Pentixafor was prepared as previously described (18-21). PET scans were acquired using an integrated PET/CT scanner (Siemens Biograph mCT 64, Siemens, Knoxville, TN, USA). Seventy-five minutes (±15 minutes) after the i.v. injection of [^{68}Ga]Pentixafor, transmission data were acquired through low-dose CT of the thorax (80 mAs, 120 kV, 512×512 matrix, slice thickness of 5 mm, increment of 30 mm/s, rotation time of 0.5 s, and pitch index of 0.8). PET emission data of the heart were then acquired in three-dimensional mode over 10 minutes. The PET data were reconstructed into a 200×200 matrix using the iterative algorithm implemented by the manufacturer, which includes decay and scatter correction based on the acquired CT data. For the control group, standard oncology imaging protocols were applied.

The images were first inspected visually by two experienced nuclear medicine physicians (CL and MK). The CT-derived number and size of enlarged mediastinal lymph nodes (med-LNs; defined as a short axis diameter>10 mm) were recorded.

For the semiquantitative analysis of increased tracer uptake, the axial PET image slice with the maximum LN uptake was selected (SUV_{max}). Tracer uptake was derived and normalized to the lean body mass and injected tracer dose. Comparisons with the noninfarcted myocardium, CMR-derived parameters (including infarct volume) and cardiovascular risk factors were performed as described previously (20).

Cardiovascular magnetic resonance imaging

All MRI scans were performed using a clinical 1.5 T scanner (Achieva 1.5 T, Philips Healthcare, Best, the Netherlands). A dedicated 32-element phased array coil was used for radiofrequency reception. All the sequences were retrospectively gated to the heart cycle via a four-lead vector cardiogram. The protocol included a morphological study based on balanced turbo field echo sequences for the documentation of standard cine long- and short-axis views (FOV 380 mm, flip angle 60°, TE 2.6-3.0 ms, TR 130-158 ms). A T2-weighted multi-echo gradient echo sequence was used for the imaging of myocardial edema in both long and short axes (FOV 370 ms, NSA 2, TE 90 ms, TR 2000-3600 ms, TR (beats) 3). For late enhancement imaging, an inversion recovery T1 turbo field echo sequence was used, and the inversion time was adjusted to completely null the myocardial signal. The sequence was performed 9 to 12 minutes after the intravenous administration of a gadolinium-based contrast agent (0.15 mmol/kg, gadobutrol, Bayer HealthCare, Leverkusen, Germany). Image analysis was performed using the Extended Workspace software (EWS, Philips Healthcare, Best, the Netherlands) and followed the standards of the Society for Cardiovascular Magnetic Resonance (23). Myocardial tissue with a signal enhancement above five standard deviations from the average normal myocardium was considered scar tissue. Analogous to the PET analyses, all LGE scans were segmentally analyzed with regard to scar distribution within the myocardium according to the 17-segment model.

Supplemental Figures:

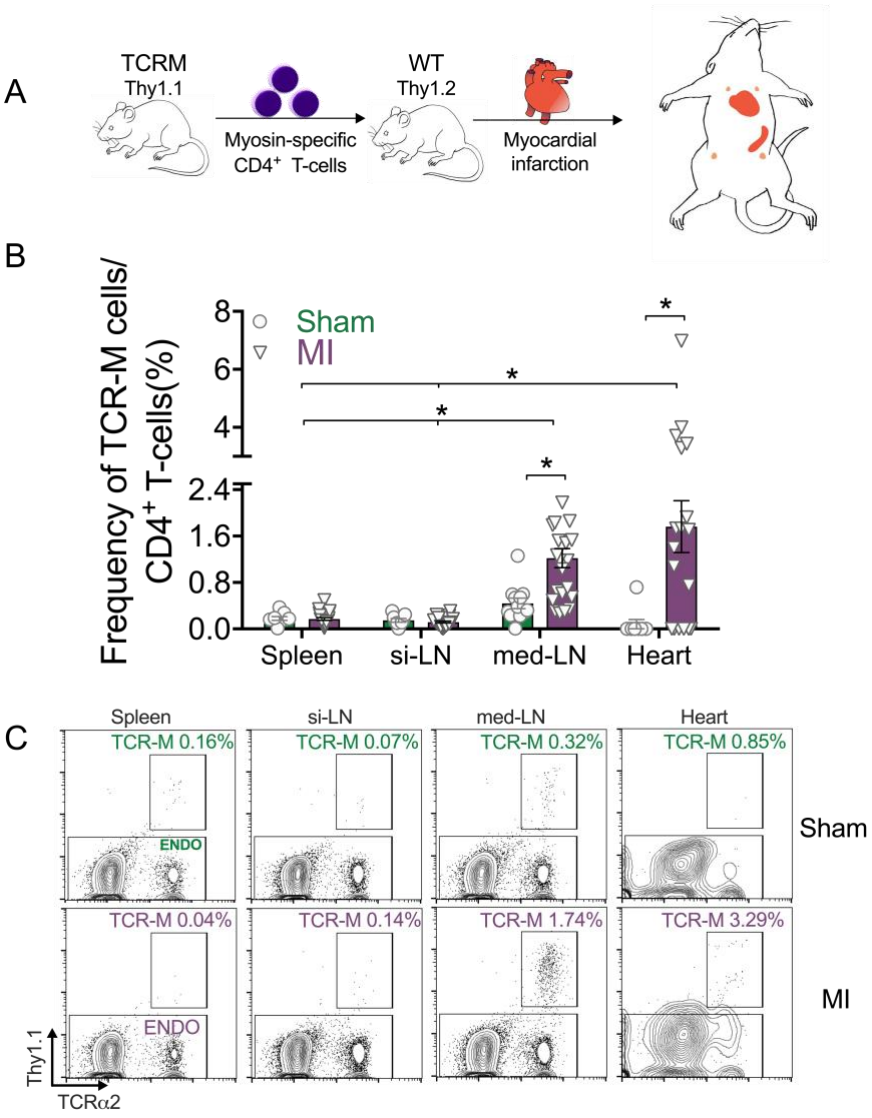

Rieckmann, et al., Supplemental Figure 1

Supplemental Figure 1: Distribution of TCR-M cells in vivo. (**A**) Experimental design and gating strategy. Thy1.1 TCR-M cells were transferred into Thy1.2 WT recipients prior to the MI or sham operation, as in Figure 2. **Panel B**: Frequencies of TCR-M found in the subiliac LNs (si-LNs), mediastinal LNs (med-LNs), heart and spleen on day 7 post-MI. This panel depicts the raw frequencies (not normalized by spleen) of the same data presented in Figure 2B. **Panel C**: Representative flow cytometry contour plots. The graphs display the group mean values (bars), the standard errors of the mean (SEMs), and the distributions of each individual value. Green and red

gridded bars represent sham- and MI-operated mice, respectively. The data were acquired in at least two independent sessions; MI (n=23) and sham (n=12). Statistical analyses: two-way ANOVA followed by Sidak's multiple comparisons test. The symbol * indicates $P<0.05$.

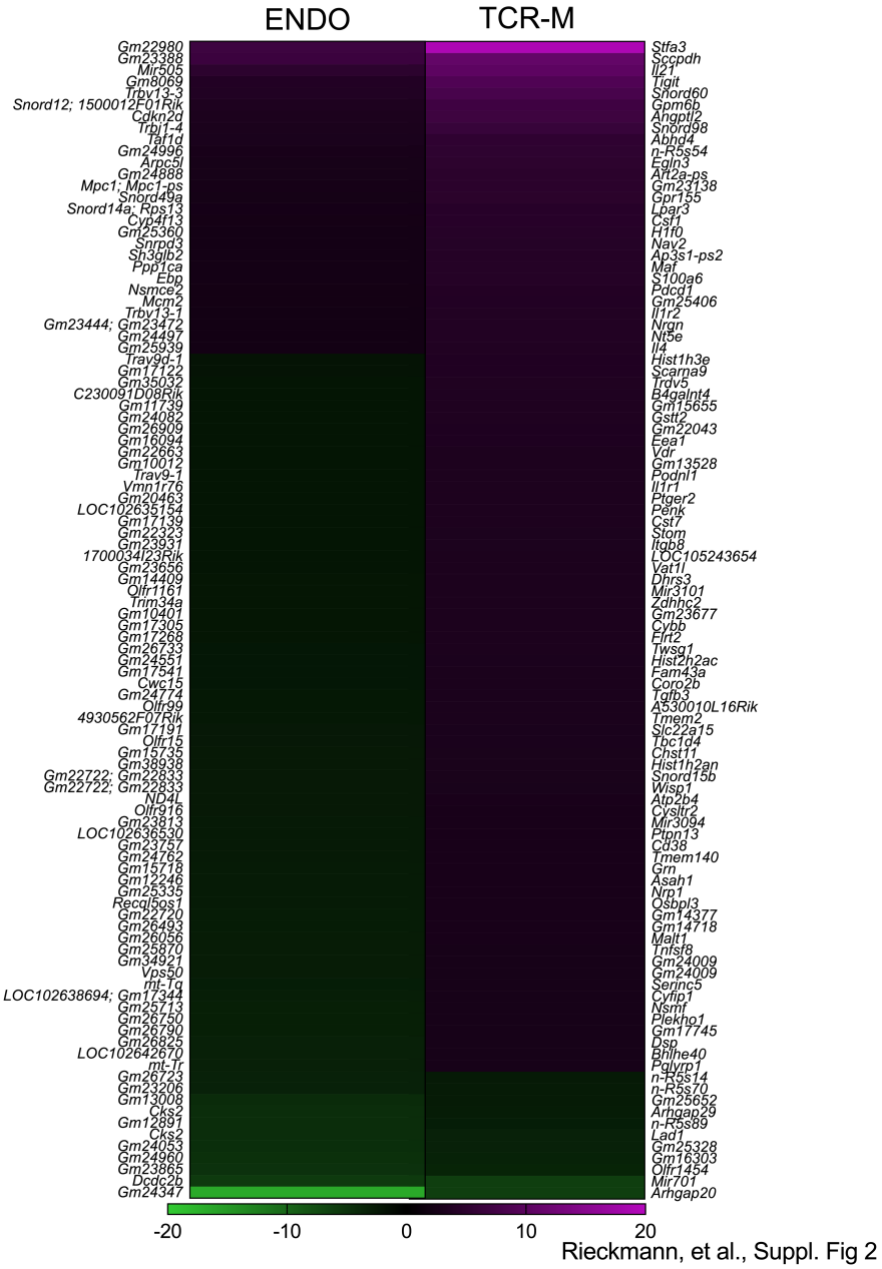

Supplemental Figure 2. Transcriptome analyses of CD4$^+$ T cells activated in the MI context.

Top 100 differentially expressed genes (MI: sham, 7 days post-MI, P<0.05) in monoclonal TCR-M cells (defined as CD4$^+$TCRβ$^+$Thy1.1$^+$TCVα2$^+$ singlets) and in polyclonal endogenous T helper cells (ENDO, defined as CD4$^+$TCRβ$^+$Thy1.1$^-$ singlets). The color scale represents the normalized gene expression (MI vs sham) in ENDO and TCR-M cells.

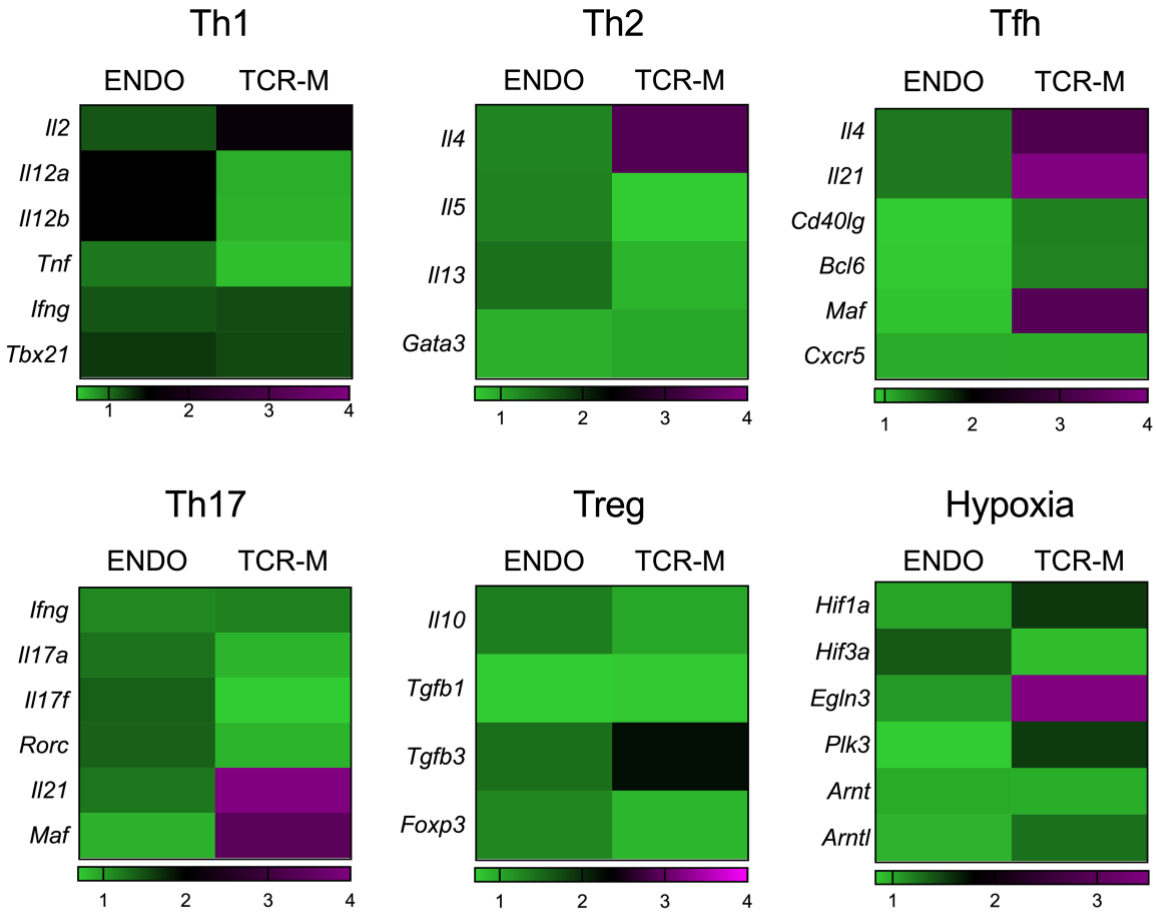

Rieckmann, et al., Suppl. Fig 3

Supplemental Figure 3 Normalized expression levels of transcripts related to all major T helper cell subsets. Th1: Type 1 T helper cells, Th2: type 2 T helper cells, Tfh: follicular T helper cells, Th17: type 17 T helper cells (Th17), and Treg: regulatory T helper cells. The color scale represents the normalized gene expression (MI vs sham) in ENDO and TCR-M cells.

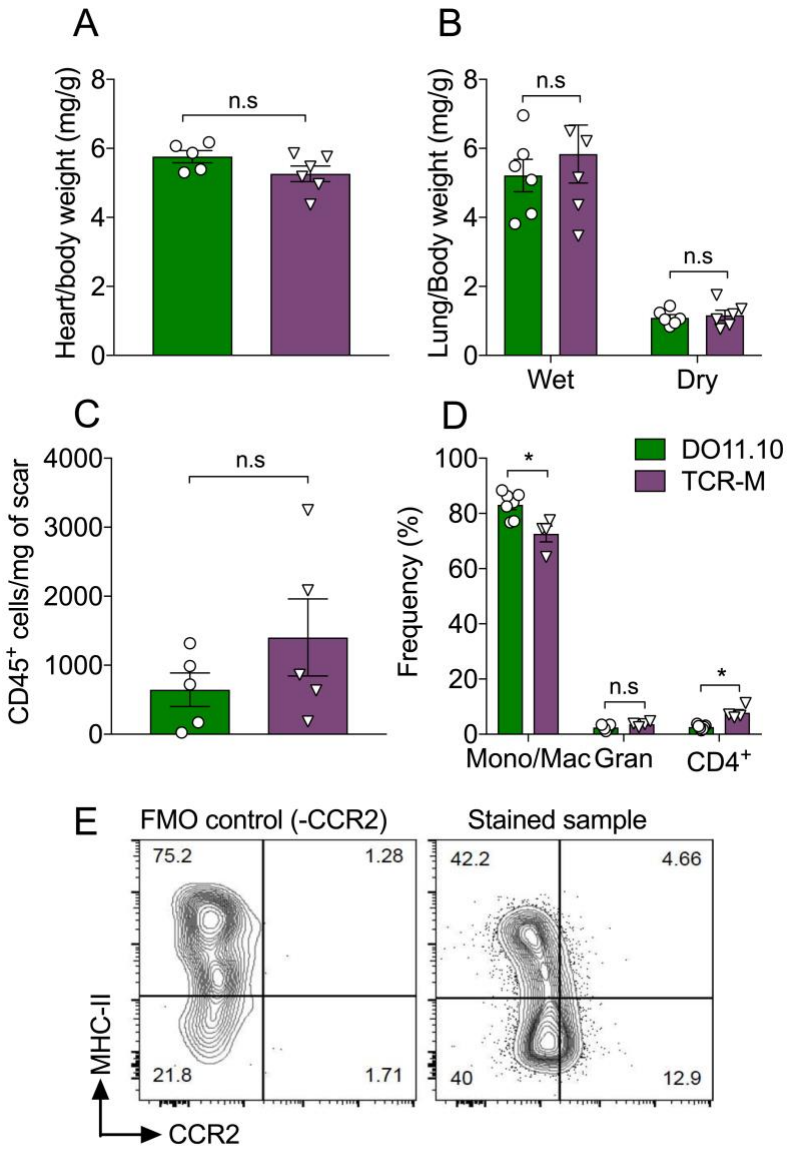

Rieckmann et al. Supp Fig 4

Supplemental Figure 4: **Organ weight and cardiac leukocytes in TCR-M transferred mice after MI.** (**A**) Normalized heart-to-body and (**B**) lung-to-body (wet and dry) weights in DO11.10- and TCR-M-transferred mice after MI (day 5 post-MI). (**C**) The cardiac leukocyte counts were normalized per mg of scar tissue analyzed days after MI. (**D**) Frequencies of monocyte/macrophages ($CD45^+$ $CD11b^+Ly6G^-$), granulocytes ($CD45^+$ $CD11b^+Ly6G^+$), and $CD4^+$ T cells ($CD45^+$ $CD11b^-Ly6G^-TCR\beta^+CD4^+$) in the infarcted heart (day 7 post-MI). (**E**) FMO controls for defining the CCR2 subsets shown in Figure 4D. The bar graphs display group mean

values (bars), standard errors of the mean (SEMs), and distributions of each sample. Statistical analysis: unpaired two-tailed T test. The symbol * indicates $P<0.05$ (DO11.10 vs TCR-M), whereas "n.s." indicates $P>0.05$.

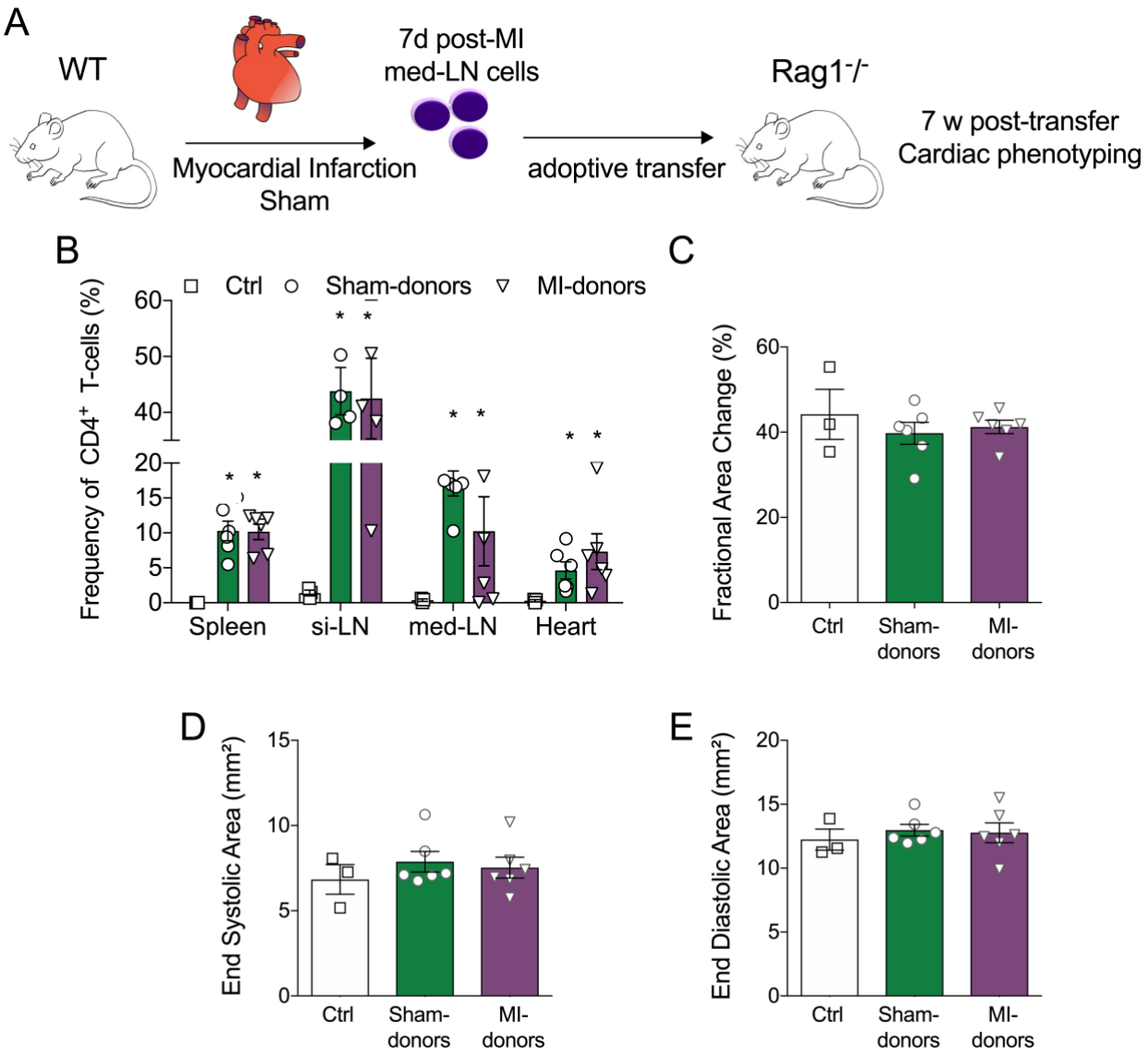

Rieckmann et al. Supp. Figure 5

Supplemental Figure 5. T helper cells activated in the MI context are not poised for a heart-destructive phenotype. (**A**) Experimental design. Med-LN cells were purified from MI- and sham-operated mice (day 7 post-MI) and then transferred into lymphocyte-deficient mice ($Rag1^{-/-}$). The cardiac function and T cell distribution were monitored 7 weeks after cell transfer. (**B**) Flow cytometry analyses of digested hearts and diverse lymphoid organs.

The fractional area change, end-systolic area, and end-diastolic area were assessed by echocardiography. The graphs in (**C)-(E**) display the group mean values (bars), the standard errors

of the mean (SEM), and the distributions of each individual value. Statistical analysis in all panels except B: one-way ANOVA followed by Dunnett's multiple comparisons test. Statistical analysis in B: two-way ANOVA followed by Sidak's multiple comparisons test). The symbol * indicates $P<0.05$ compared with the Ctrl group (no transfer). No difference was observed between the sham and MI donors. The data for MI recipients (n=6), sham recipients (n=6) and controls receiving no adoptive transfer (n=3) from one session are shown.

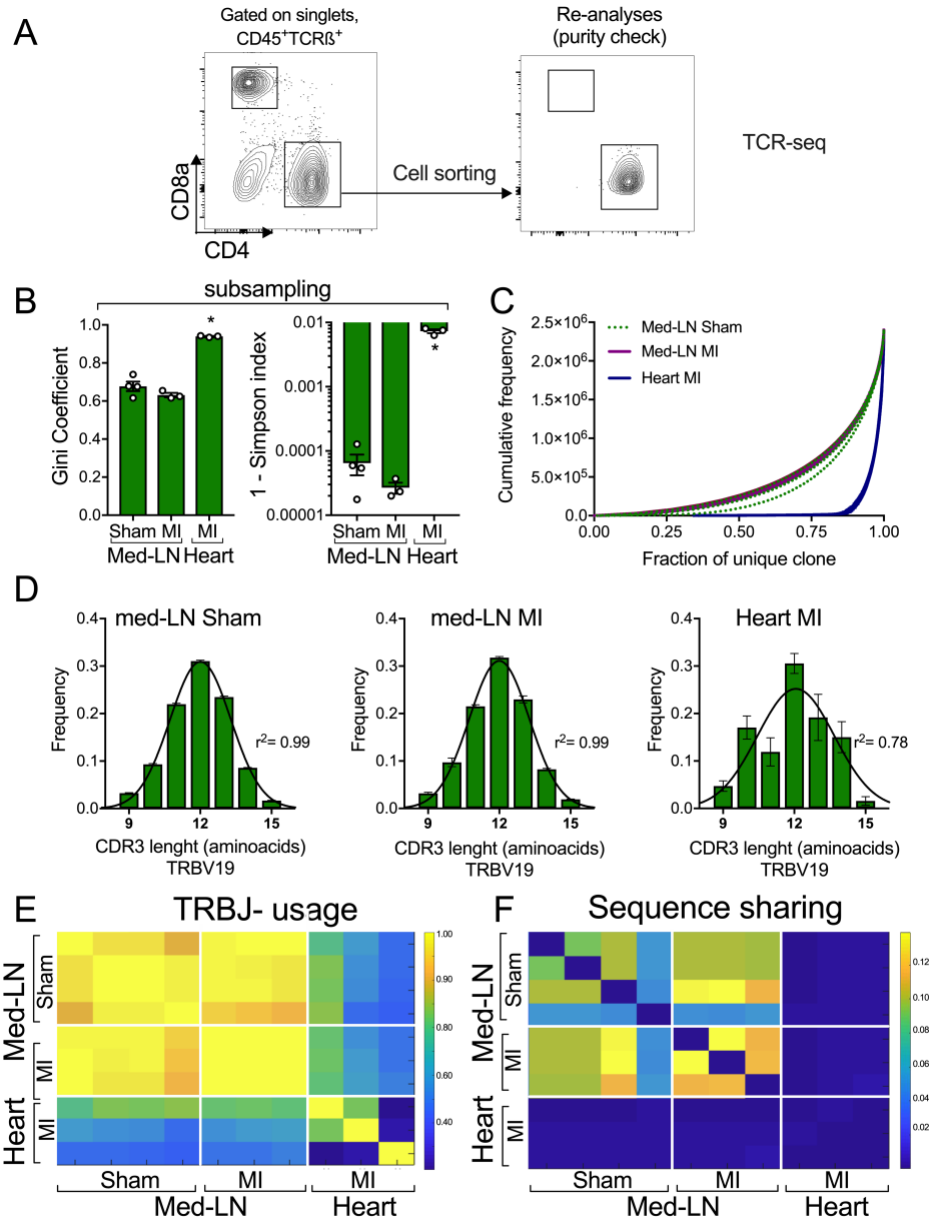

Rieckmann, et al., Supplemental Figure 6

Supplemental Figure 6. MI-induced changes in the TCR repertoire. (**A**) T helper cells ($CD4^+$ $TCR\beta^+$ $CD8^-$) were FACS-purified from the heart and med-LNs of MI and sham-operated mice (day 7). Only samples with >98% purity were used for downstream molecular analyses. (**B**) Gini coefficient of repertoire evenness and 1-Simpson's diversity index assessed in a subsample of equal size. (**C**) Lorenz curves of each individual sample. (**D**) Distribution of TRBV19 CDR3 length in

all groups, showing a biased TRBV19 spectratyping in the cardiac T cell repertoire compared with a Gaussian length distribution in med-LNs. (**E**) Heat map depicting the correlation in the frequencies of J-gene segments between all sample pairs. (**F**) Heat map depicting the overlap (Jaccard index) of CDR3 sequences between any two given subsamples of equal size. In **B-C**, the group mean values (bars), the standard error of the mean (SEM) of 3- 4 samples per group, and the distribution of each individual value are shown. Statistical analyses: One-way ANOVA followed by Dunnett's multiple comparison test. The symbol * indicates a P value < 0.05 compared to all other groups.

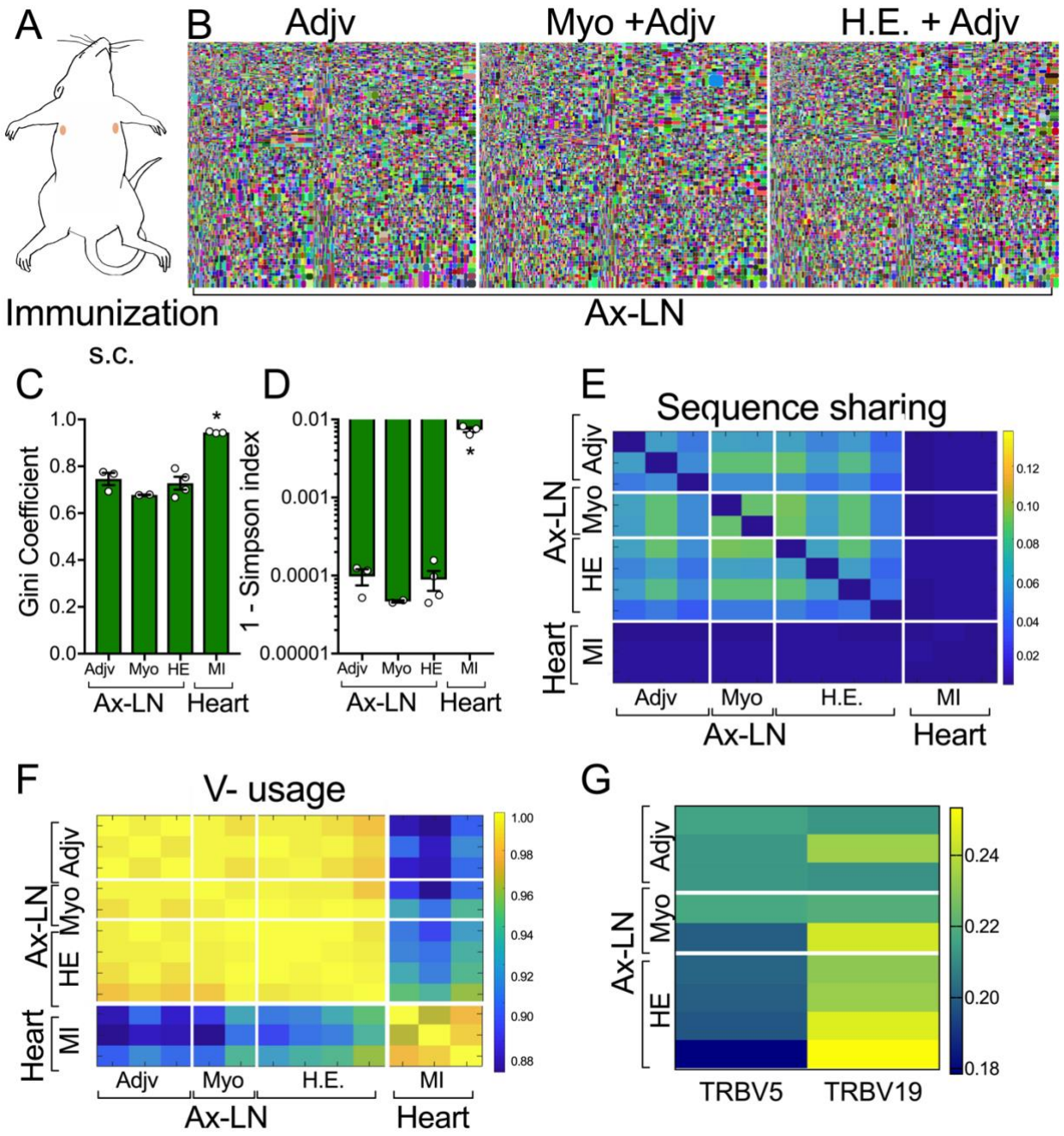

Rieckmann, et al., Supplemental Figure 7

Supplemental Figure 7. T cell responses to MI and to immunization with cardiac antigen show minimal repertoire overlap. (**A**) $CD4^+$ $TCR\beta^+$ $CD8^-$ cells were purified from the ax-LNs of mice receiving s.c. immunization with cardiac myosin, heart extract or adjuvant alone (Titermax

Gold). (**B**) Tree maps depicting repertoire evenness and diversity. (**C**) Gini coefficient of repertoire evenness. (**D**) 1-Simpson's diversity index. (**E**) Sequence sharing (Jaccard index) between any two samples (bulk repertoire). (**F**) Heat map depicting the correlation in frequencies of the V-gene segments between all sample pairs. (**G**) Frequency of TRBV5 and TRBV19 among the immunization groups.

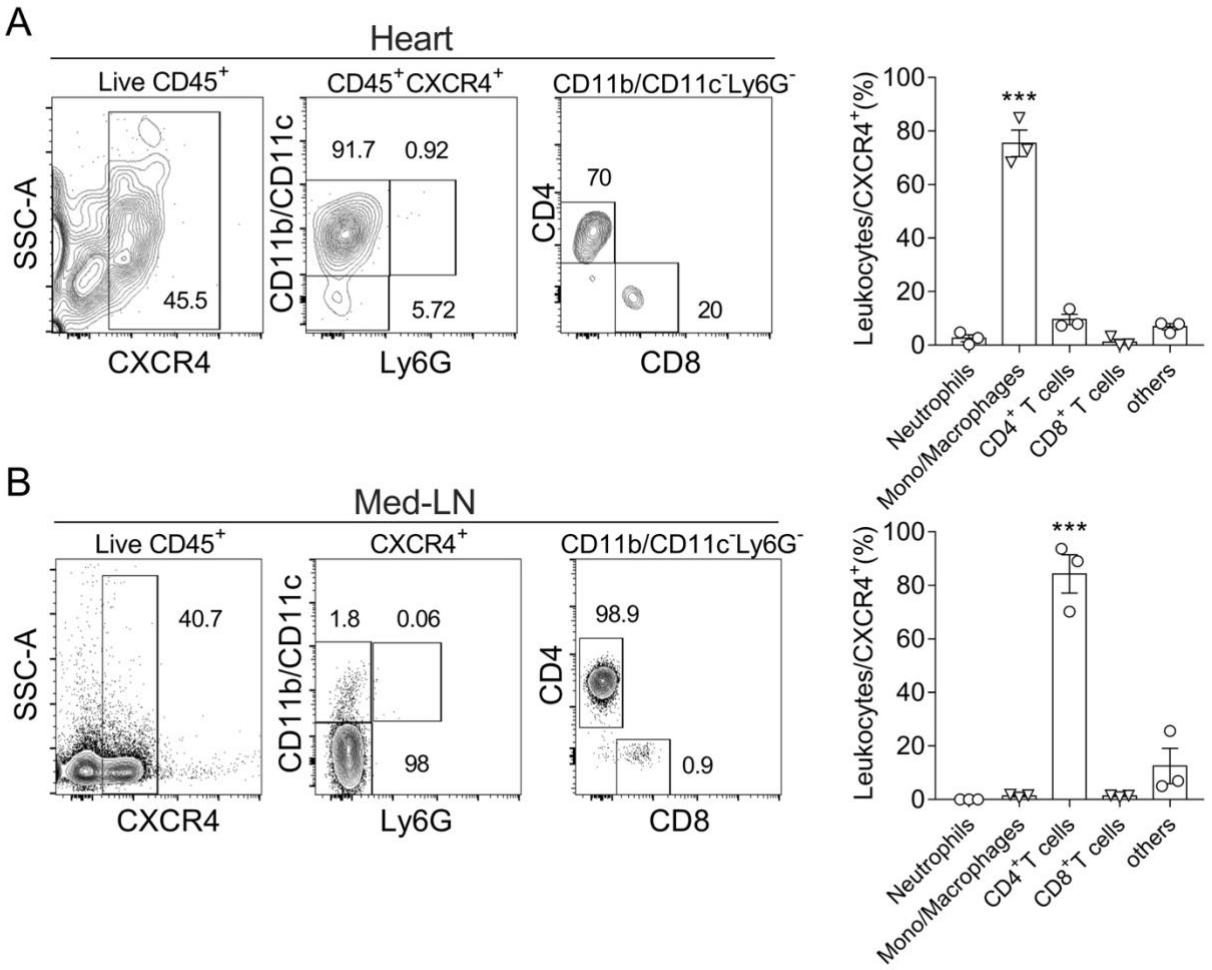

Rieckmann et al. Supp Fig 8

Supplemental Figure 8: Distribution of heart and med-LN leukocytes within the CXCR4$^+$ population. (**A**) Gating strategy illustrates the analysis of main leukocyte populations within CXCR4$^+$ cells in healthy hearts. The graph depicts the frequency of neutrophils (CD45$^+$CD11b$^+$Ly6G$^+$), monocytes/macrophages (CD45$^+$CD11b$^+$Ly6G$^-$), CD4$^+$ T cells (CD45$^+$CD11b/CD11c$^-$Ly6G$^-$CD4$^+$) and CD8$^+$ T cells (CD45$^+$CD11b/CD11c$^-$Ly6G-CD8$^+$). (**B**) Gating strategy and graph indicate the frequency of the respective leukocyte population within CXCR4$^+$ cells in med-LNs of healthy mice (n:3). Statistical analysis: One-way ANOVA followed by Dunnett's multiple comparison test. The symbol *** indicates a *P* value < 0.01 compared to all groups.

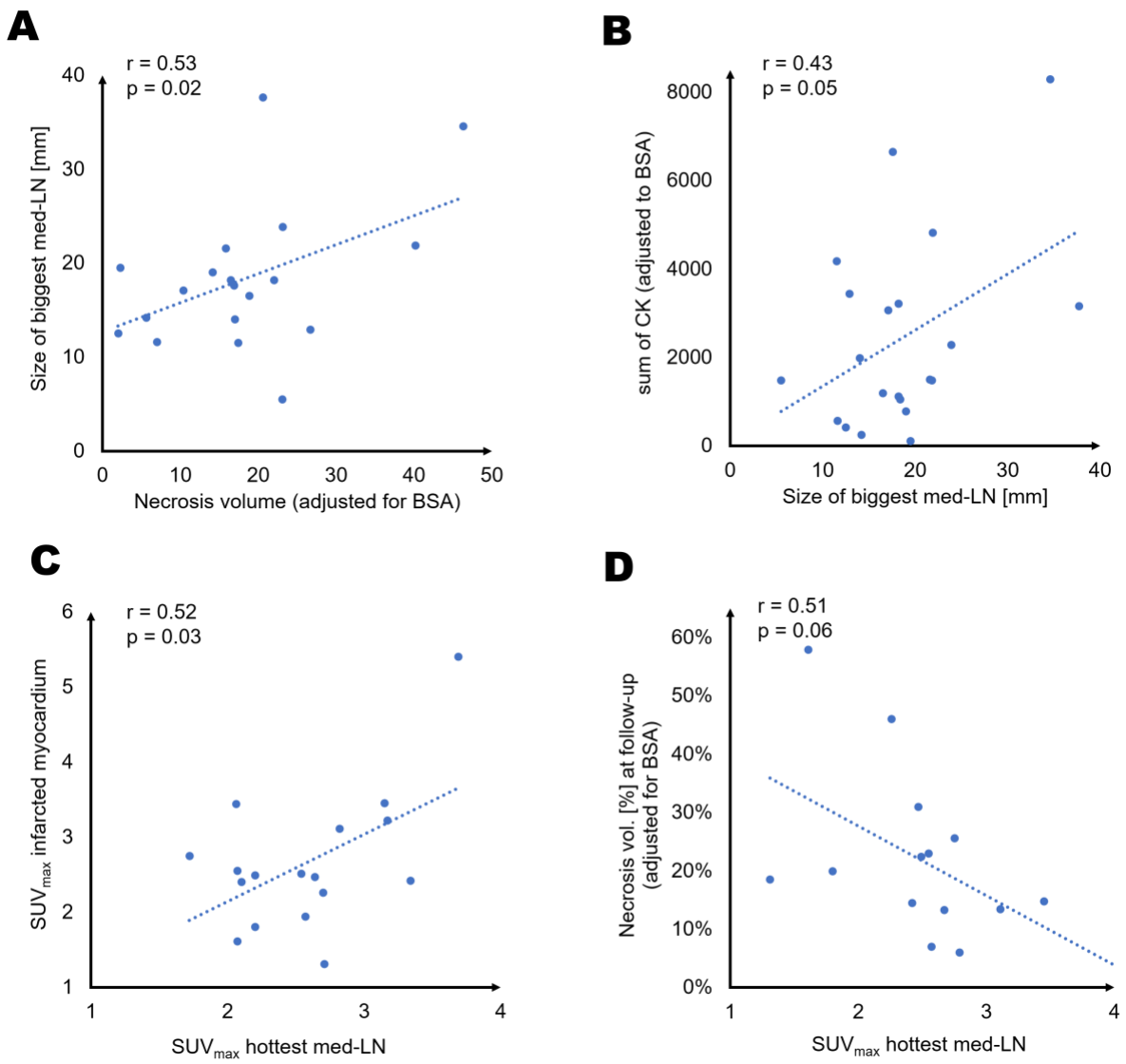

Supplemental Figure 9. The med-LN morphology and T cellularity show a moderate correlation with infarct size and outcome. (**A**) Correlations between med-LN morphology and necrosis volume (derived from CT and CMR measurements, respectively). (**B**) Correlation between med-LN morphology and plasma creatinine kinase levels (sum of CK levels). (**C**) Correlation between CXCR4 signal levels (SUVmax) in the infarcted myocardium and med-LNs. (**D**)**:** Correlation between CXCR4 expression levels (SUVmax) and necrosis volume at follow-up measurements performed 4 months (median) after MI. The exact correlation coefficients (r) and P values are indicated in each graph.

Table S1: List of MHC-II-restricted peptides derived from the major heart-specific proteins tested.

Haplotype	$Protein_{pepide}$	Pepide sequence	Percentile Rank (%)
	ACTC1		
I-A^d	$ACTC1_{132-146}$	PAMYVAIQAVLSLYA	0.03
I-A^d	$ACTC1_{173-187}$	LPHAIMRLDLAGRDL	2.48
I-A^d	$ACTC1_{223-237}$	LDFENEMATAASSSS	8.00
I-A^d	$ACTC1_{312-326}$	ADRMQKEITALAPST	1.04
I-A^d	$ACTC1_{319-333}$	ITALAPSTMKIKIIA	4.75
I-A^d	$ACTC1_{323-337}$	APSTMKIKIIAPPER	4.16
I-A^d	$ACTC1_{352-366}$	STFQQMWISKQEYDE	8.23
	ADRB1		
I-A^d	$ADRB1_{24-39}$	GAATAARLLVLASPP	1.76
I-A^d	$ADRB1_{95-111}$	FIMSLASADLVMGLL	2.63
I-A^d	$ADRB1_{142-157}$	TASIETLCVIALDRY	3.60
I-A^d	$ADRB1_{144-160}$	SIETLCVIALDRYLA	3.19
I-A^d	$ADRB1_{164-178}$	FRYQSLLTRARARAL	1.22
I-A^d	$ADRB1_{166-181}$	YQSLLTRARARALVC	5.46
I-A^d	$ADRB1_{174-188}$	TRARARALVCTVWAI	4.27

I-A^{d}	ADRB1$_{177-193}$	RARALVCTVWAISAL	3.10
I-A^{d}	ADRB1$_{179-194}$	RALVCTVWAISALVS	2.20
I-A^{d}	ADRB1$_{182-196}$	VCTVWAISALVSFLP	1.35
I-A^{d}	ADRB1$_{303-318}$	ALREQKALKTLGIIM	0.23
I-A^{d}	ADRB1$_{380-394}$	CCARRAACRRRAAHG	1.61
	MYBPC3		
I-A^{d}	MYBPC3$_{15-29}$	KPRSAEVTAGSAAVF	6.25
I-A^{d}	MYBPC3$_{17-31}$	RSAEVTAGSAAVFEA	5.03
I-A^{d}	MYBPC3$_{18-32}$	SAEVTAGSAAVFEAE	8.47
I-A^{d}	MYBPC3$_{57-71}$	LAAEGKRHTLTVRDA	3.62
I-A^{d}	MYBPC3$_{60-74}$	EGKRHTLTVRDASPD	0.86
I-A^{d}	MYBPC3$_{171-185}$	VFSARVAGASLLKPP	5.34
I-A^{d}	MYBPC3$_{210-224}$	SYDRASKVYLFELHI	4.57
I-A^{d}	MYBPC3$_{265-279}$	LRSAFRRTSLAGAGR	7.66
I-A^{d}	MYBPC3$_{266-281}$	RSAFRRTSLAGAGRRT	3.54
I-A^{d}	MYBPC3$_{268-283}$	AFRRTSLAGAGRRTSD	5.08
I-A^{d}	MYBPC3$_{370-384}$	QVNKGHKIRLTVELA	6.66
I-A^{d}	MYBPC3$_{374-388}$	GHKIRLTVELADPDA	2.27

I-A^{d}	MYBPC3$_{411-425}$	VGAKRTLTISQCSLA	6.69
I-A^{d}	MYBPC3$_{412-427}$	GAKRTLTISQCSLADD	8.08
I-A^{d}	MYBPC3$_{453-467}$	TRSLEDQLVMVGQRV	6.27
I-A^{d}	MYBPC3$_{916-929}$	LQGLTERRSMLVKDL	1.84
I-A^{d}	MYBPC3$_{919-933}$	LTERRSMLVKDLPTG	0.30
I-A^{d}	MYBPC3$_{932-946}$	TGARLLFRVRAHNVA	9.52
I-A^{d}	MYBPC3$_{834-848}$	EGVAYEMRVYAVNAV	0.98
I-A^{d}	MYBPC3$_{835-849}$	GVAYEMRVYAVNAVG	1.02
I-A^{d}	MYBPC3$_{833-847}$	IEGVAYEMRVYAVNA	2.37
I-A^{d}	MYBPC3$_{827-841}$	HEARRMIEGVAYEMR	4.04
I-A^{d}	MYBPC3$_{756-770}$	DQVNLTVKVIDVPDA	4.49
I-A^{d}	MYBPC3$_{757-771}$	QVNLTVKVIDVPDAP	5.03
I-A^{d}	MYBPC3$_{542-556}$	EVYQSIADLAVGAKD	4.60
I-A^{d}	MYBPC3$_{537-551}$	QEKKLEVYQSIADLA	4.92
I-A^{d}	MYBPC3$_{543-557}$	VYQSIADLAVGAKDQ	5.04
I-A^{d}	MYBPC3$_{533-547}$	ELIVQEKKLEVYQSI	5.19
I-A^{d}	MYBPC3$_{544-558}$	YQSIADLAVGAKDQA	7.05
I-A^{d}	MYBPC3$_{624-638}$	KLHFMEVKIDFVPRQ	5.68

I-A^{d}	MYBPC3$_{973-987}$	RHLRQTIQKKVGEPV	6.92
I-A^{d}	MYBPC3$_{1047-1061}$	NMEDKATLILQIVDK	4.08
I-A^{d}	MYBPC3$_{1046-1060}$	ENMEDKATLILQIVD	4.64
I-A^{d}	MYBPC3$_{1183-1197}$	LANRSIIAGYNAILC	9.15
I-A^{d}	MYBPC3$_{1223-1237}$	FRMFCKQGVLTLEIR	4.90
	MYHCA		
I-A^{d}	MYHCA$_{1-15}$	MTDAQMADFGAAAQY	5.6
I-A^{d}	MYHCA$_{41-56}$	DKEEYVKAKVVSREG	1.79
I-A^{d}	MYHCA$_{86-100}$	KIEDMAMLTFLHEPA	6.04
I-A^{d}	MYHCA$_{105-119}$	LKERYAAWMIYTYSG	6.78
I-A^{d}	MYHCA$_{131-145}$	LPVYNAEVVAAYRGK	5.69
I-A^{d}	MYHCA$_{186-201}$	VNTKRVIQYFASIAA	4.25
I-A^{d}	MYHCA$_{190-204}$	RVIQYFASIAAIGDRS	3.42
I-A^{d}	MYHCA$_{191-205}$	VIQYFASIAAIGDRS	2.73
I-A^{d}	MYHCA$_{216-231}$	LEDQIIQANPALEAF	9.18
I-A^{d}	MYHCA$_{420-434}$	QVYYSIGALAKSVYE	2.46
I-A^{d}	MYHCA$_{605-619}$	TVVGLYQKSSLKLMA	9.10
I-A^{d}	MYHCA$_{608-622}$	GLYQKSSLKLMATLF	1.55

I-A^{d}	MYHCA$_{609-623}$	LYQKSSLKLMATLFS	0.98
I-A^{d}	MYHCA$_{610-624}$	YQKSSLKLMATLFST	1.20
I-A^{d}	*MYHCA$_{614-628}$	SLKLMATLFSTYASA	9.04
I-A^{d}	MYHCA$_{641-655}$	KKGSSFQTVSALHRE	5.64
I-A^{d}	MYHCA$_{642-656}$	KGSSFQTVSALHREN	7.20
I-A^{d}	MYHCA$_{720-734}$	FRQRYRILNPAAIPE	2.13
I-A^{d}	MYHCA$_{721-735}$	RQRYRILNPAAIPEG	4.00
I-A^{d}	MYHCA$_{722-736}$	QRYRILNPAAIPEGQ	2.13
I-A^{d}	MYHCA$_{776-790}$	EEMRDERLSRIITRI	9.91
I-A^{d}	MYHCA$_{777-791}$	EMRDERLSRIITRIQ	7.57
I-A^{d}	MYHCA$_{778-792}$	MRDERLSRIITRIQA	5.05
I-A^{d}	MYHCA$_{781-795}$	ERLSRIITRIQAQAR	7.80
I-A^{d}	MYHCA$_{786-801}$	IITRIQAQARGQLMRI	7.08
I-A^{d}	MYHCA$_{793-807}$	QARGQLMRIEFKKIV	9.50
I-A^{d}	MYHCA$_{810-824}$	RDALLVIQWNIRAFM	8.21
I-A^{d}	MYHCA$_{814-828}$	LVIQWNIRAFMGVKN	4.57
I-A^{d}	MYHCA$_{815-829}$	VIQWNIRAFMGVKNW	3.38
I-A^{d}	MYHCA$_{833-847}$	KLYFKIKPLLKSAET	9.13

I-A^{d}	MYHCA$_{910-924}$	LIKNKIQLEAKVKEM	8.97
I-A^{d}	MYHCA$_{911-925}$	IKNKIQLEAKVKEMT	7.40
I-A^{d}	MYHCA$_{994-1008}$	LTKEKKALQEAHQQA	5.89
I-A^{d}	MYHCA$_{996-1010}$	KEKKALQEAHQQALD	5.26
I-A^{d}	MYHCA$_{1000-1014}$	ALQEAHQQALDDLQA	4.42
I-A^{d}	MYHCA$_{1003-1017}$	EAHQQALDDLQAEED	2.63
I-A^{d}	MYHCA$_{1039-1053}$	SLEQEKKVRMDLERA	4.18
I-A^{d}	MYHCA$_{1040-1054}$	LEQEKKVRMDLERAK	2.54
I-A^{d}	MYHCA$_{1044-1058}$	KKVRMDLERAKRKLE	4.45
I-A^{d}	MYHCA$_{1124-1138}$	LEAERTARAKVEKLR	2.40
I-A^{d}	MYHCA$_{1126-1140}$	AERTARAKVEKLRSD	2.55
I-A^{d}	MYHCA$_{1183-1197}$	ATLQHEATAAALRKK	3.04
I-A^{d}	MYHCA$_{1185-1199}$	LQHEATAAALRKKHA	2.21
I-A^{d}	MYHCA$_{1231-1245}$	DDVTSNMEQIIKAKA	3.20
I-A^{d}	MYHCA$_{1235-1249}$	SNMEQIIKAKANLEK	1.18
I-A^{d}	MYHCA$_{1238-1252}$	EQIIKAKANLEKVSR	7.20
I-A^{d}	MYHCA$_{1258-1272}$	ANEYRVKLEEAQRSL	3.96
I-A^{d}	MYHCA$_{1259-1273}$	NEYRVKLEEAQRSLN	3.67

I-A^{d}	MYHCA$_{1290-1304}$	ARQLEEKEALISQLT	7.55
I-A^{d}	MYHCA$_{1293-1307}$	LEEKEALISQLTRGK	8.74
I-A^{d}	MYHCA$_{1326-1340}$	KAKNALAHALQSSRH	7.27
I-A^{d}	MYHCA$_{1327-1341}$	AKNALAHALQSSRHD	9.00
I-A^{d}	MYHCA$_{1350-1364}$	EEEMEAKAELQRVLS	2.52
I-A^{d}	MYHCA$_{1351-1365}$	EEMEAKAELQRVLSK	2.48
I-A^{d}	MYHCA$_{1388-1402}$	LEEAKKKLAQRLQDA	5.96
I-A^{d}	MYHCA$_{1391-1405}$	AKKKLAQRLQDAEEA	3.10
I-A^{d}	MYHCA$_{1394-1408}$	KLAQRLQDAEEAVEA	5.32
I-A^{d}	MYHCA$_{1397-1411}$	QRLQDAEEAVEAVNA	2.09
I-A^{d}	MYHCA$_{1401-1415}$	DAEEAVEAVNAKCSS	5.43
I-A^{d}	MYHCA$_{1435-1449}$	ERSNAAAAALDKKQ	2.00
I-A^{d}	MYHCA$_{1470-1484}$	ESSQKEARSLSTELF	7.68
I-A^{d}	MYHCA$_{1471-1485}$	SSQKEARSLSTELFK	4.21
I-A^{d}	MYHCA$_{1528-1542}$	EKIRKQLEVEKLELQ	2.97
I-A^{d}	MYHCA$_{1530-1544}$	IRKQLEVEKLELQSA	4.42
I-A^{d}	MYHCA$_{1539-1553}$	VEKLELQSALEEAEA	4.75
I-A^{d}	MYHCA$_{1567-1582}$	NQIKAEIERKLAEKD	6.53

I-A^{d}	MYHCA$_{1589-1605}$	RNHLRMVDSLQTSLD	4.31
I-A^{d}	MYHCA$_{1621-1635}$	GDLNEMEIQLSQANR	0.80
I-A^{d}	MYHCA$_{1623-1637}$	LNEMEIQLSQANRIA	0.59
I-A^{d}	MYHCA$_{1651-1688}$	HLKDTQLQLDDAVHA	7.48
I-A^{d}	MYHCA$_{1652-1686}$	LKDTQLQLDDAVHAN	6.67
I-A^{d}	MYHCA$_{1752-1766}$	NAEEKAKKAITDAAM	2.63
I-A^{d}	MYHCA$_{1782-1796}$	ERMKKNMEQTIKDLQ	7.74
I-A^{d}	MYHCA$_{1783-1797}$	RMKKNMEQTIKDLQH	6.04
I-A^{d}	MYHCA$_{1808-1823}$	GGKKQLQKLEARVRE	2.62
I-A^{d}	MYHCA$_{1809-1824}$	GKKQLQKLEARVREL	5.02
I-A^{d}	MYHCA$_{1868-1882}$	LVDKLQLKVKAYKRQ	1.15
	MYL2		
I-A^{d}	MYL2$_{113-127}$	SLKADYVREMLTTQA	5.24
I-A^{d}	MYL2$_{118-132}$	DYVREMLTTQAERFS	0.90
I-A^{d}	MYL2$_{120-134}$	REMLTTQAERFSKEE	5.68
	TNNI3		
I-A^{d}	TNNI3$_{19-33}$	VRRRSSANYRAYATE	6.02
I-A^{d}	TNNI3$_{32-46}$	TEPHAKKKSKISASR	5.12

I-A^{d}	TNNI3$_{34-48}$	EPHAKKKSKISASRK	3.40
I-A^{d}	TNNI3$_{40-54}$	SKISASRKLQLKTLM	3.81
I-A^{d}	TNNI3$_{44-58}$	ASRKLQLKTLMLQIA	1.20
I-A^{d}	TNNI3$_{45-59}$	SRKLQLKTLMLQIAK	1.91
I-A^{d}	TNNI3$_{50-64}$	LKTLMLQIAKQEMER	4.27
I-A^{d}	TNNI3$_{97-111}$	LCRQLHARVDKVDEE	9.00
I-A^{d}	TNNI3$_{140-154}$	FKRPTLRRVRISADA	6.71
I-A^{d}	TNNI3$_{144-158}$	TLRRVRISADAMMQA	0.18
I-A^{d}	TNNI3$_{146-161}$	RRVRISADAMMQALL	0.10
I-A^{d}	TNNI3$_{150-165}$	ISADAMMQALLGTRA	0.22
I-A^{d}	TNNI3$_{152-166}$	ADAMMQALLGTRAKE	1.28
I-A^{d}	TNNI3$_{160-176}$	LGTRAKESLDLRAHL	1.39
I-A^{d}	TNNI3$_{163-177}$	RAKESLDLRAHLKQV	7.06
I-A^{d}	TNNI3$_{164-178}$	AKESLDLRAHLKQVK	6.50
	TNNT2		
I-A^{d}	TNNT2$_{226-240}$	AERRKALAIDHLNED	1.23
	HSPB3		
I-A^{d}	HSPB3$_{1-15}$	MAKIILRHLIETPVR	7.34

I-A^{d}	HSPB3$_{71-85}$	GKSRFQILLDVVQFL	4.06

ACTC1: alpha actin, cardiac muscle 1; ADRB1: adrenergic receptor beta 1; MYBPC3: myosin-ending protein C3; MYHCA: myosin heavy chain alpha; MYL2: myosin light chain 2; TNNI3: troponin I3; TNNT2: troponin T2; HSPB3: heat-shock protein family member 3. For each peptide, a percentile rank was calculated based on three different MHC-II prediction methods (combinatorial library, SMM_align and Sturniolo) after comparing the peptide's score against the scores of five million random 15 mers selected from SWISSPROT database. A small numbered percentile rank indicates high MHC-II binding affinity (in silico prediction tool: IEDB, 6).

Table S II. Enriched Pathways according to the NCI-Nature Database.

	TCR-M MI vs Sham			
Description	**P value**	**Adjusted P value**	**Z-score**	**combined score**
Sphingosine 1-phosphate (S1P) pathway	0.0009018	0.05761	-1.20	8.38
TCR signaling in naive $CD4^+$ T cells	0.002866	0.05761	-1.57	9.22
HIF-1-alpha transcription factor network	0.003205	0.05761	-1.28	7.34
PAR4-mediated thrombin signaling events	0.008170	0.1085	-0.52	2.49
Endothelins	0.02032	0.1844	-1.39	5.41
Validated targets of C-MYC transcriptional repression	0.02032	0.1844	-1.27	4.94
LPA receptor-mediated events	0.02206	0.1844	-1.46	5.56
VEGFR1 specific signals	0.02541	0.1844	-0.65	2.37
Glypican 1 network	0.02541	0.1844	-0.42	1.55
AP-1 transcription factor network	0.02577	0.1844	-1.32	4.84

IL2 signaling events mediated by STAT5	0.03094	0.2055	-0.51	1.76
IL1-mediated signaling events	0.03688	0.2287	-0.48	1.58

ENDO MI vs Sham

Description	**P value**	**Adjusted P value**	**Z-score**	**combined score**
ALK1 signaling events	0.1321	0.2639	-1.40	2.84
ATR signaling pathway	0.1984	0.2639	-1.37	2.22
BMP receptor signaling	0.2120	0.2639	-1.34	2.09
TGF-beta receptor signaling	0.2639	0.2639	-1.49	1.98

Table S III. Gene Ontology analysis according to molecular function.

	TCR-M MI vs Sham			
Description	**P value**	**Adjusted P value**	**Z-score**	**combined score**
Macrophage colony-stimulating factor receptor binding (GO:0005157)	0.002905	0.3840	-1.18	6.91
Chemokine receptor binding (GO:0042379)	0.003205	0.3840	-2.34	13.46
Interleukin-4 receptor binding (GO:0005136)	0.006143	0.3840	-1.55	7.87
Transforming growth factor beta binding (GO:0050431)	0.01046	0.3840	-1.59	7.26
G-protein beta/gamma-subunit complex binding (GO:0031683)	0.01046	0.3840	-1.55	7.05
Interleukin-1 receptor activity (GO:0004908)	0.01169	0.3840	-1.72	7.66
Opioid receptor binding (GO:0031628)	0.01348	0.3840	-2.12	9.12
Growth factor activity (GO:0008083)	0.02296	0.3840	-2.10	7.94

Phosphatidylinositol-4,5-bisphosphate 3-kinase activity (GO:0046934)	0.02388	0.3840	-2.19	8.18
protein tyrosine phosphatase activity (GO:0004725)	0.03192	0.3840	-2.14	7.37

ENDO MI vs Sham

Description	**P value**	**Adjusted P value**	**Z-score**	**combined score**
U7 snRNA binding (GO:0071209)	0.04432	0.3204	-1.01	3.16
U2 snRNA binding (GO:0030620)	0.04973	0.3204	-0.82	2.45

Table S IV. Description of patients from whom cardiac autopsies were obtained

	Control (*n*=9)	MI (*n*=23)				
		Early phase (*n*=6)	Inflam. phase (*n*=9)	Prol. phase (*n*=8)	*P* value	MI vs. control P value
Age (years)	62±18	62±18	66±7	60±9	0.59*	0.85**
Male sex	6 (67)	5 (83)	8 (89)	6 (67)	0.17	0.65
Medical history						
Previous MI	0 (0)	5 (83)	2 (22)	4 (44)	0.07	0.02
Diabetes mellitus type II	0 (0)	0 (0)	1 (11)	2 (22)	0.44	0.55
Peripheral arterial disease	1 (11)	1 (17)	1 (11)	1 (11)	0.94	>0.99
Cerebral vascular accident	1 (11)	0 (0)	1 (11)	0 (0)	0.42	0.48
Chronic kidney disease	0 (0)	0 (0)	0 (0)	1 (11)	0.42	>0.99
Chronic obstructive pulmonary disease	2 (22)	0 (0)	0 (0)	1 (11)	0.42	0.17

Cancer	1 (11)	2 (33)	0 (0)	3 (33)	0.15	>0.99
Successful percutaneous coronary intervention	0 (0)	0 (0)	5 (56)	1 (11)	0.03	0.16
Primary reason of death						
Myocardial infarction	-	6 (100)	9 (100)	9 (100)	-	-
Arrythmia	-	4 (67)	2 (22)	3 (33)	0.21	-
Heart failure	-	1 (17)	3 (33)	3 (33)	0.74	-
Vital bleeding	-	1 (17)	2 (22)	1 (11)	0.82	-
Other/unknown	-	0 (0)	2 (22)	2 (22)	0.45	-
Arrhythmia (not associated with MI)	1 (11)	-	-	-	-	- -
Acute aortic rupture/ dissection	4 (44)	-	-	-	-	- -
Acute large pulmonary embolism	1 (11)	-	-	-	-	- -
Respiratory insufficiency	1 (11)	-	-	-	-	- -
Trauma	2 (22)	-	-	-	-	- -

Table S V. Description of patients enrolled in the PET-CT imaging study.

Description	Control (n=5)	MI (n=22)
Male	3 (66)	17 (77)
Age [years]	59±8	61±12
LVEF [%]	N/A	50±10
Pain to balloon time [h]	-	9±7
Quantity of diseased vessels		
1 vessel	-	13 (59)
2 vessels	-	3 (14)
3 vessels	-	7 (32)
Infarct vessel		
Left marginal artery	-	0
Left anterior artery	-	10 (45)
Left circumflex artery	-	3 (14)
Right coronary artery	-	9 (41)
TIMI flow		

III	-	11 (50)
II	-	10 (45)
0 - I	-	2 (2)
Laboratory results		
CRP (mg/dL)	0.22±0.21	0.87±2.63
CK max [U/L]	N/A	2419±2541
CKMB max [U/L]	N/A	207±226
TnT max, [pg/ml]	N/A	2626±4047
LDH [U/L]	N/A	726±434

The values represent the mean ± mean standard deviation. LVEF: left ventricular ejection fraction (%). CRP: C-Reactive Protein. CK: creatine kinase, CKMB: creatine kinase muscle brain. TnT: troponin T. LDH: Lactate dehydrogenase.

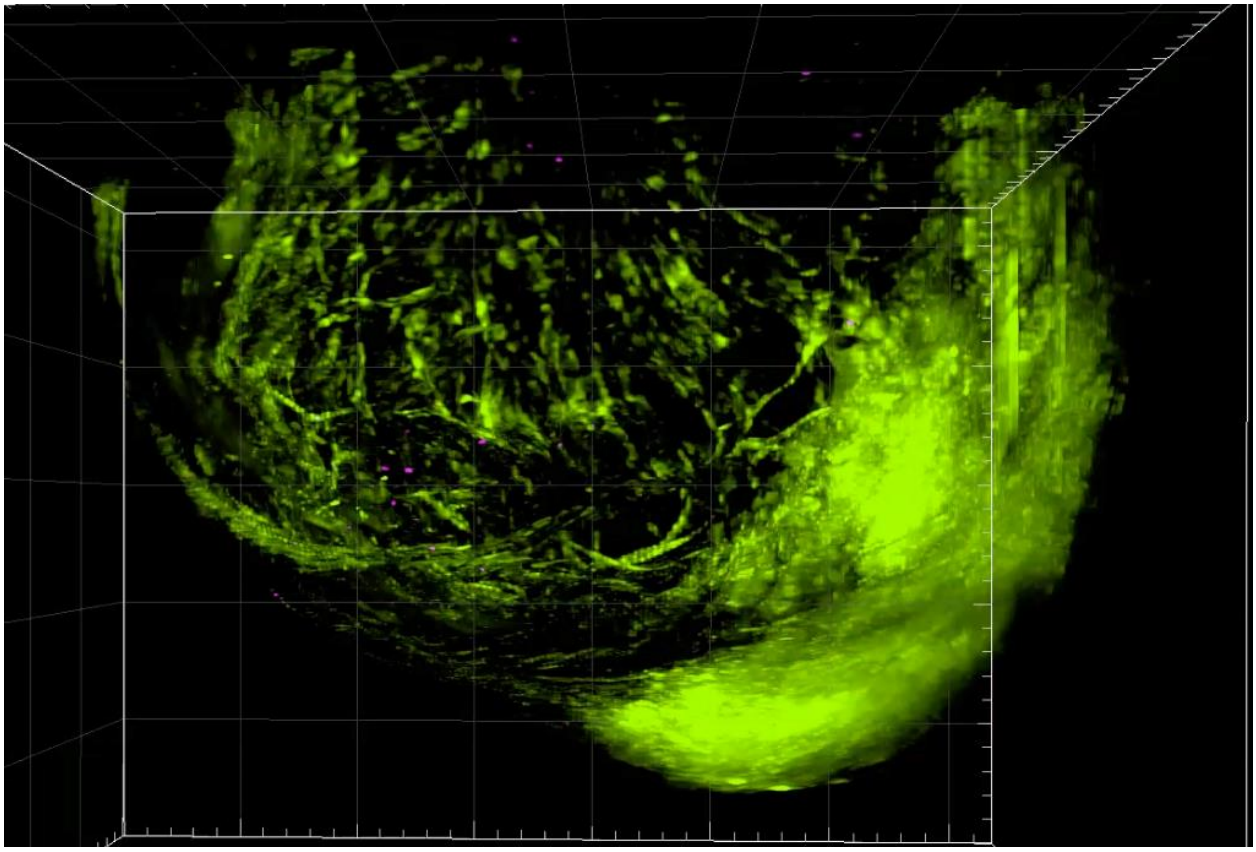

Still image from Movie S1. 3D reconstructions of infarcted hearts performed by means of light-sheet fluorescence microscopy (LSFM) reveal the accumulation of myosin-specific T helper cells at 7 days post-MI. Morphological information was acquired based on the autofluorescence levels in the green channel. The viable myocardium appears in bright green, whereas the necrotic myocardium appears in dark green. TCR-M cells (Thy1.1^{+}) appear in magenta (5x magnification).

1. Nindl V, Maier R, Ratering D, De Giuli R, Zust R, Thiel V, et al. Cooperation of Th1 and Th17 cells determines transition from autoimmune myocarditis to dilated cardiomyopathy. *Eur J Immunol.* 2012;42(9):2311-21.
2. Hofmann U, Beyersdorf N, Weirather J, Podolskaya A, Bauersachs J, Ertl G, et al. Activation of CD4+ T lymphocytes improves wound healing and survival after experimental myocardial infarction in mice. *Circulation.* 2012;125(13):1652-63.
3. Weirather J, Hofmann UD, Beyersdorf N, Ramos GC, Vogel B, Frey A, et al. Foxp3+ CD4+ T cells improve healing after myocardial infarction by modulating monocyte/macrophage differentiation. *Circ Res.* 2014;115(1):55-67.
4. Uhlen M, Fagerberg L, Hallstrom BM, Lindskog C, Oksvold P, Mardinoglu A, et al. Proteomics. Tissue-based map of the human proteome. *Science.* 2015;347(6220):1260419.
5. Apweiler R, Bairoch A, Wu CH, Barker WC, Boeckmann B, Ferro S, et al. UniProt: the Universal Protein knowledgebase. *Nucleic Acids Res.* 2004;32(Database issue):D115-9.
6. Wang P, Sidney J, Dow C, Mothe B, Sette A, and Peters B. A systematic assessment of MHC class II peptide binding predictions and evaluation of a consensus approach. *PLoS Comput Biol.* 2008;4(4):e1000048.
7. Karulin AY, Quast S, Hesse MD, and Lehmann PV. Neuroantigen-Specific CD4 Cells Expressing Interferon-gamma (IFN-gamma), Interleukin (IL)-2 and IL-3 in a Mutually Exclusive Manner Prevail in Experimental Allergic Encephalomyelitis (EAE). *Cells.* 2012;1(3):576-96.
8. Ramos GC, van den Berg A, Nunes-Silva V, Weirather J, Peters L, Burkard M, et al. Myocardial aging as a T-cell-mediated phenomenon. *Proc Natl Acad Sci U S A.* 2017;114(12):E2420-E9.

9. Burzyn D, Kuswanto W, Kolodin D, Shadrach JL, Cerletti M, Jang Y, et al. A special population of regulatory T cells potentiates muscle repair. *Cell.* 2013;155(6):1282-95.
10. Chen EY, Tan CM, Kou Y, Duan Q, Wang Z, Meirelles GV, et al. Enrichr: interactive and collaborative HTML5 gene list enrichment analysis tool. *BMC Bioinformatics.* 2013;14:128.
11. Kuleshov MV, Jones MR, Rouillard AD, Fernandez NF, Duan Q, Wang Z, et al. Enrichr: a comprehensive gene set enrichment analysis web server 2016 update. *Nucleic Acids Res.* 2016;44(W1):W90-7.
12. Brede C, Friedrich M, Jordan-Garrote AL, Riedel SS, Bauerlein CA, Heinze KG, et al. Mapping immune processes in intact tissues at cellular resolution. *J Clin Invest.* 2012;122(12):4439-46.
13. Vogel B, Siebert H, Hofmann U, and Frantz S. Determination of collagen content within picrosirius red stained paraffin-embedded tissue sections using fluorescence microscopy. *MethodsX.* 2015;2:124-34.
14. Ramos GC, Dalbo S, Leite DP, Goldfeder E, Carvalho CR, Vaz NM, et al. The autoimmune nature of post-infarct myocardial healing: oral tolerance to cardiac antigens as a novel strategy to improve cardiac healing. *Autoimmunity.* 2012;45(3):233-44.
15. Madi A, Shifrut E, Reich-Zeliger S, Gal H, Best K, Ndifon W, et al. T-cell receptor repertoires share a restricted set of public and abundant CDR3 sequences that are associated with self-related immunity. *Genome Res.* 2014;24(10):1603-12.
16. Madi A, Poran A, Shifrut E, Reich-Zeliger S, Greenstein E, Zaretsky I, et al. T cell receptor repertoires of mice and humans are clustered in similarity networks around conserved public CDR3 sequences. *Elife.* 2017;6.

17. van der Laan AM, Ter Horst EN, Delewi R, Begieneman MP, Krijnen PA, Hirsch A, et al. Monocyte subset accumulation in the human heart following acute myocardial infarction and the role of the spleen as monocyte reservoir. *Eur Heart J.* 2014;35(6):376-85.
18. Lapa C, Kircher S, Schirbel A, Rosenwald A, Kropf S, Pelzer T, et al. Targeting CXCR4 with [(68)Ga]Pentixafor: a suitable theranostic approach in pleural mesothelioma? *Oncotarget.* 2017;8(57):96732-7.
19. Lapa C, Luckerath K, Kleinlein I, Monoranu CM, Linsenmann T, Kessler AF, et al. (68)Ga-Pentixafor-PET/CT for Imaging of Chemokine Receptor 4 Expression in Glioblastoma. *Theranostics.* 2016;6(3):428-34.
20. Lapa C, Luckerath K, Rudelius M, Schmid JS, Schoene A, Schirbel A, et al. [68Ga]Pentixafor-PET/CT for imaging of chemokine receptor 4 expression in small cell lung cancer--initial experience. *Oncotarget.* 2016;7(8):9288-95.
21. Reiter T, Kircher M, Schirbel A, Werner RA, Kropf S, Ertl G, et al. Imaging of C-X-C Motif Chemokine Receptor CXCR4 Expression After Myocardial Infarction With [(68)Ga]Pentixafor-PET/CT in Correlation With Cardiac MRI. *JACC Cardiovasc Imaging.* 2018.
22. Heinze B, Fuss CT, Mulatero P, Beuschlein F, Reincke M, Mustafa M, et al. Targeting CXCR4 (CXC Chemokine Receptor Type 4) for Molecular Imaging of Aldosterone-Producing Adenoma. *Hypertension.* 2018;71(2):317-25.
23. Schulz-Menger J, Bluemke DA, Bremerich J, Flamm SD, Fogel MA, Friedrich MG, et al. Standardized image interpretation and post processing in cardiovascular magnetic resonance: Society for Cardiovascular Magnetic Resonance (SCMR) board of trustees task force on standardized post processing. *J Cardiovasc Magn Reson.* 2013;15:35.